UNIVERSITA' DEGLI STUDI DI PADOVA

DIPARTIMENTO DI FISICA "GALILEO GALILEI"

CORSO DI LAUREA IN FISICA

TESI DI LAUREA TRIENNALE

VOIDS AND THE LARGE-SCALE STRUCTURE OF THE UNIVERSE

Laureanda:

Valentina Picciano

Relatore:

Prof. Sabino Matarrese

ANNO ACCADEMICO 2016-2017

Contents

1 Introduction

The Cosmic Web represents the spatial organization of matter on large scale, approximately on the order of hundred of Megaparsec(1). It defines a complex spatial pattern of intricate connected structures where the distribution of matter is non-uniform, in fact matter is arranged in dense regions with clusters, elongated filaments and sheet like walls and low density regions practically devoid of any bright galaxies called voids. The analysis of the Cosmic Web is one of the most interesting way to investigate the distribution of galaxies and dark matter on the largest scales of the Universe.
In this thesis we analyse every aspect of the Cosmic Web, from the descriptions of its components such as filaments, walls and voids to the methods designed to detect such voids, giving particular attention to the principal approaches to estimate density fields from a particle distribution: the Delaunay and the Voronoi tessellations.
Cosmic Voids are the major components of the large scale Universe, since they continue increasing their dimensions dominating the volume of the Universe, while, on the contrary, rich dense regions increase in density but not in volume. Voids are regions with sizes of $20 - 50h^{-1}\,Mpc$(2), usually with a roundish shape (in fact, they can never be perfectly spherical) surrounded by filaments, walls and clusters of galaxies. Although the geometry of Cosmic Voids with all of their subcomponents have been studied and analysed for many years, since the first galaxy surveys were compiled, today their observation is still very difficult, first of all because we have not got a standard definition of them, then because studying voids means estimating density fields from a particle distribution. Generally there are two substantially different methods to extract topological information from a discrete set of points, each of them is based on computer simulations of the density field that has to be studied; on one hand all the problems of a direct observation are avoided, but on the other hand we have a simulated Universe and it is possible that unobservable information can not be applied to the observed Universe. Nevertheless, these methods are considered both valid to a first approximation:

- N-body simulations.
- Delaunay and Voronoi tessellations.

The Delaunay and the Voronoi tessellations are the basis of two void finders, two different algorithms that find density depressions in a set of points; these two methods are called: Zobov and the Watershed Void Finder (WVF). Although they pursue the same purpose, the WVF is defined with respect to the Delaunay Tessellation Field Estimator (DTFE), whereas the Zobov algorithm is defined with respect to the Voronoi tessellation, so they have different characteristics, whose we evaluate pros and contros.
This thesis is laid out as follows: in the First Chapter we introduce the Cosmic Web, giving the reasons of the birth of such an intricate pattern in the distribution of matter and

(1) Parsec is a unit of length used to evaluate large distances of objects outside the Solar system.
$1\,pc = 3.26\,ly$
$1\,Mpc = 10^6\,pc$

(2) Mpc denotes large galactic distances, such as the one between two galaxies, and it is usually expressed in units of $\frac{Mpc}{h}$, where $h = 67.8 \pm 0.9$[1] is a parameter that gives the uncertainty of the Hubble constant H for the rate of expansion of the Universe.

$$h = \frac{H}{100\,kms^{-1}Mpc^{-1}}$$

describing its components; then in the Third Chapter we focus on the Voids, deepening some aspects such as their shape, evolution and dynamics with respect to the cosmic background; in the Fourth Chapter we explain in detail the Voronoi and the Delaunay tessellations, useful in the description of the WVF and the ZOBOV methods of detecting voids.

2 Cosmic Web

On the largest scales of the Universe the distribution of matter is non-uniform and due the gravitational instability is organized into an intricate network of connected structures known as *Cosmic Web*.
This complicate geometry of the Universe has been known since the first galaxy redshift surveys were observed, lately the improvement of methods such as cosmological N-body simulations and Bayesan reconstructions of the distribution of dark matter in the Local Universe demonstrate an even more intricate pattern.
Although it is nearly impossible to give a rigid mathematical treatment of the features of the Cosmic Web, it is convenient to introduce some approximations. First of all, suppose that the Cosmic Web is characterized by discrete features such as galaxies and clusters, black holes and pulsars, objects that provide a direct link to the early epochs of the Universe; although all these features derive from a direct observation of the Cosmos, the most prominent components of the Cosmic Web are considered the filaments.
Filaments have the size of 10 up to 100 Mpc[4], they provide a connection between regions with highest density and magnitude within the texture of the Cosmic Web, called knots; filaments are channels through which mass flows and then clusters.
Moreover, there are two objects in the pattern of the Cosmic Web that play a key role: walls and voids.
Walls are sheet-like membranes with low overdensity matter, they are populated by dwarf galaxies or galaxies with low magnitude and as a consequence their observation is still very difficult.
Voids are large underdense region practically devoid of any galaxy occupying the major volume of the Universe, in that sense these objects provide a pristine environment for the study of the primordial Universe. The first observation of voids and, consequently, an evidence for their existence was found in galaxy redshift studies, moreover the discovery of the Boötes void by Kirshner et al.[2] and the CfA study by de Lapparent et al.[3] established them as key aspects of the large scale galaxy distribution.
Since the study of the web-like pattern combined with the analysis of the matter evolution in the early epochs of the Universe has always been a cosmological aim, different methods have been designed in order to pursue this study. The largest N-body simulation done thus far is the *Millennium Run* or *Millennium Simulation*, a computer simulation that used over ten billion particles to trace the evolution of the distribution of matter in a cubic region of a simulated Universe over 2 billion light-years on a side. In Figure 1 it is possible to see slices of this simulated Universe at four different epochs, each frame has a size of $31.25h^{-1}$ Mpc and zooms in on the central cluster.

2.1 Evolution and dynamics of the Cosmic Web

The intricate Megaparsec web-like pattern is the greatest example of complex geometry where the distribution of matter reaches a non-linear stage due to the gravitational instability.
The evolution of the Universe can be understood if we suppose two different epochs.

- Early Universe. The initial density field is nearly a homogeneous and isotropic Gaussian random field. This epoch is dominated by a linear matter fluctuations.
- Epoch of the CMB emission. It is the epoch of the non-linearity, we see the growth of large underdense regions as much as the growth of long filamentary structures.

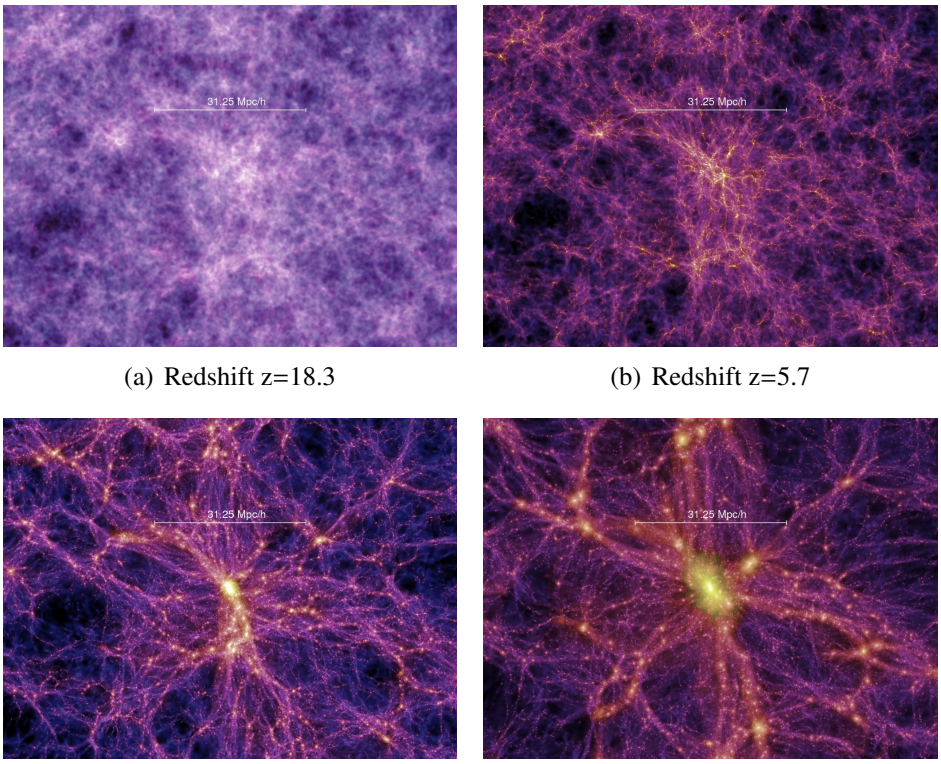

(a) Redshift z=18.3 (b) Redshift z=5.7

(c) Redshift z=1.4 (d) Redshift z=0

Figure 1: Frames of the Millennium Simulation of the ΛCDM taken at four different epochs of the Universe highlight the evolution of the distribution of matter after the Big Bang due to the gravitational clustering as well as the intricate pattern of the Cosmic Web. Observable are knots, the filamentary geometry and then walls and voids, underdense regions[4].

In the latter period, a general density fluctuation field for a region of the Universe with respect to the cosmic background mass density ρ_u can be written as follows:

$$\delta(\vec{r}, t) = \frac{\rho(\vec{r}) - \rho_u}{\rho_u}$$

where $\delta(\vec{r}, t)$ is also called *density contrast*.
When $\delta \neq 0$, so when that region of the Universe has a different mass density with respect to the cosmic background, there is the presence of a gravitational acceleration $\vec{g}(\vec{r}, t)$ that can be written as the integration over space of all the gravitational attraction exerted by all matter fluctuations of the Universe.

$$\vec{g}(\vec{r}, t) = -4\pi G \rho_m(t) a(t)^2 \int \delta(\vec{r'}, t) \frac{(\vec{r} - \vec{r'})}{(\vec{r} - \vec{r'})^3} \, \mathrm{d}\vec{r'}$$

where $\rho_m(t)$ is the mean density of the mass in the Universe, G is the gravitational constant and $a(t)$ is the scale factor.
The expression of the gravitational acceleration comes from the relation: $\vec{g} = -\frac{\nabla\Phi}{a}$ and the Poisson-Newton equation of the gravitational potential

$$\nabla^2\Phi = 4\pi G \rho_m(t) a(t)^2 \delta(\vec{r}, t)$$

Also the Hubble parameter H and the density parameter Ω_m, two of the main cosmological parameters, are related to the equation of the gravitational acceleration.

Following the laws of the Newton Mechanics, the equation of motion of an isolated sphere of radius R in the approximation of an isotropic and expanding universe is

$$\frac{d^2\vec{R}(t)}{dt^2} = -\frac{GM}{\vec{R}(t)^2}$$

Multiplying both side of the equation above for $\frac{d\vec{R}(t)}{dt}$ and integrating, this differential equation can be written as

$$\frac{1}{2}\left(\frac{d\vec{R}(t)}{dt}\right)^2 = \frac{GM}{\vec{R}(t)} + K \tag{1}$$

Mathematically, K is just a constant of integration, but in a physical sense it represents the total energy of the expanding sphere. The radius of the expanding sphere $\vec{R}(t)$ is replaced with $a(t)r$ where a(t), as seen before, is the expansion factor and r is the comoving radius, the physical radius at the epoch where $a(t_0)=1$. Moreover the sphere's mass is $M = \frac{4\pi}{3} r^3 \rho(t) a(t)^3$.
Eq.(1) can be rewritten as

$$\frac{1}{2} r^2 \dot{a}(t)^2 = \frac{4\pi}{3} G r^2 \rho(t) a(t)^2 + K$$

and then

$$\left(\frac{\dot{a}(t)}{a(t)}\right)^2 = \frac{8\pi}{3} G\rho(t) + \frac{2K}{a(t)^2 r^2} \tag{2}$$

This equation describes not just an isolated sphere, but all spherical volumes in a homogeneous and isotropic Universe because of the approximation of a spherical symmetry.
In the case of the General Relativity the form of the Eq.(2) is:

$$\left(\frac{\dot{a}(t)}{a(t)}\right)^2 = \frac{8\pi}{3} G\rho(t) - \frac{kc^2}{r^2}\frac{1}{a(t)^2}$$

With the introduction of the Hubble parameter $H(t) = \frac{\dot{a}(t)}{a(t)}$ and the approximation of $k = 0$ (the approximation of a flat universe in a ΛCDM scenario), the equation becomes

$$H(t)^2 = \frac{8\pi}{3} G\rho_c(t)$$

Hence, it is possible to extract the value of the critical density $\rho_c(t) = \frac{3H(t)^2}{8\pi G}$ and introduce the density parameter Ω used in cosmology to describe the energy density of the Universe, $\Omega = \bar{\rho}_m \frac{8\pi G}{3H(t)^2}$. Now, we have the equation that links together the cosmological density parameter and the gravitational acceleration $\vec{g}(\vec{r}, t)$:

$$\vec{g}(\vec{r}, t) = -\frac{3}{2} H(t)^2 \Omega(t) a(t) \int \delta(\vec{r'}, t) \frac{(\vec{r} - \vec{r'})}{(\vec{r} - \vec{r'})^3} \, \mathrm{d}r'$$

The consequence of the presence of a gravitational acceleration is a perturbation of the matter flows and that implies a perturbation of the velocity field.

$$\vec{u}(\vec{r}, t) = \frac{da(t)\vec{r}}{dt} = H(t)a(t)\vec{r} + \vec{v}(\vec{r}, t)$$

The equation of motion for these velocity perturbations comes from a recasting of the Euler equation of fluid dynamics, so

$$\frac{\partial \vec{u}}{\partial t} + \left(\vec{u} \cdot \vec{\nabla}\right) \vec{u} = \vec{g}$$

in GR becomes

$$\frac{\partial \vec{v}}{\partial t} + \frac{\dot{a}}{a}\vec{v} + \frac{1}{a}\left(\vec{v} \cdot \vec{\nabla}\right) \vec{v} = -\frac{1}{a} \nabla \Phi$$

In this process, the mass conservation is guaranteed by the Continuity equation:

$$\frac{\partial \delta}{\partial t} + \frac{1}{a} \nabla \cdot (1 + \delta)\, \vec{v} = 0$$

The continuity equation shows how in large overdense region around density peaks the gravitational attraction slows down the expansion of matter relative to the mean of the background, whereas in large underdense region the expansion is faster. So in those regions when the density is higher, the expansion arrives to a halt and then the matter starts to infall and collapse on itself. This explains the birth of the characteristic structures of the Cosmic Web.

3 Cosmic Voids

The study of cosmic voids starts with the observation and the analysis of the first galaxy surveys and with the discovery of the first dramatic specimen: the *Boötes Void*, the emptiest region in the known Universe. This void is an almost spherical region of space about 250 million light years in diameter and contains just few galaxies. Since that discovery, voids have been considered the main features of the Cosmic Web with a key role in the spatial organization of matter in the Universe.

- Voids are a prominent aspect in the Megaparsec Universe, since they are regions with size of $20 - 50h^{-1}\,Mpc$ with the lowest density mass that occupy the major volume of the Universe. In fact, thanks to recent statistical analysis, such as the Millennium Simulation, upon the morphological components of the Cosmic Web in a ΛCDM scenario, scientists have come to the awareness that voids are around the 77% of the cosmic volume and contain the 15% of the mass fraction. As a consequence, voids have an average density of 20% of the Universe average density, as illustrated in Figure 2

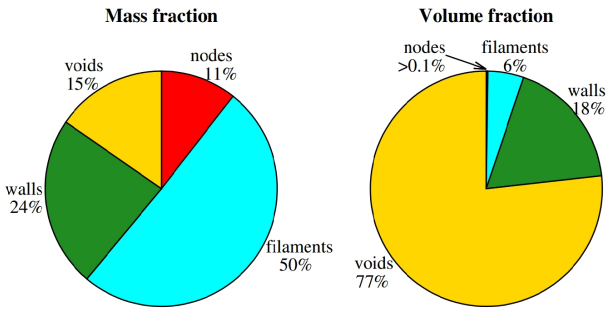

Figure 2: Mass and volume fractions occupied by the cosmic web features detected by the NEXUS+ method[6].

- Voids can be also a test of the cosmological parameters and of the ΛCDM theory because of the lack of dwarf galaxies inside them.
  The ΛCDM theory is the standard model of cosmology; it is based upon the approximation of a flat Universe whose main feature is the presence of cold dark matter, where cold stands for a non-collisional and non-baryonic matter that is indeed supposed to be constituted by Weakly Interacting Massive Particles (WIMP); moreover, another main feature of this theoretical model is the presence of dark energy represented by the cosmological constant Λ; atoms and photons constitute just the 5% of the cosmic matter.

- Their pristine environment is useful for the study of the formation of the first objects and the evolution of matter distribution.

It is impossible to have a satisfying knowledge of the Cosmic Web without comprehending the structure and the evolution of voids.

3.1 Formation and evolution of Voids

As already said, the reason of the main difficulties in the studying and the cataloguing of voids is the lack of an objective definition of them.
Generally voids' sizes depend on the magnitude of the galaxies used to define them: if we consider a L_* galaxy, voids defined by galaxies brighter than L_* usually have diameters of 10-20h^{-1} Mpc[7], whereas voids with less luminous galaxies are larger. Although mini-voids and super-sized voids have already been seen in simulations, theoretical calculations do not provide an upper or lower limit in voids' dimension.
Voids are manifestation of the cosmic structure formation reaching a non-linear stage of evolution, but where do they originate?
The density fluctuations of the primordial Gaussian field formed density troughs, nursery of the first voids. From theoretical models we understand that as a consequence of their underdensity, the gravity is weaker inside them than in other part of the Universe, this causes an outflow of matter due to an effective repulsive force; in other words, the matter streams out of the void faster than the Hubble flow.(3)
As matter streams out of the void, on one hand the void reaches an internal uniformity while density decreases, on the other hand the matter accumulates outside the void where the flow becomes slower and we see the birth of long filaments, tenuous walls and populated knots. This is what happens in a theoretical spherical and isolated voids; the reality in some ways is similar to this approximation. In the figure below there are six frames representing the evolution of a spherical void based on a simulation in a ΛCDM scenario.
The first step is the outflow of matter from the interior of the void towards the outline. A spherical isolated void would asymptotically reach an underdensity of δ=-1, however, in the reality, several factors affect the evolution of voids. As the mass flows out of the underdense region, the void becomes increasingly uniform and the matter accumulates around its edges where the gravitational acceleration decreases and the main features of the Cosmic Web start forming.

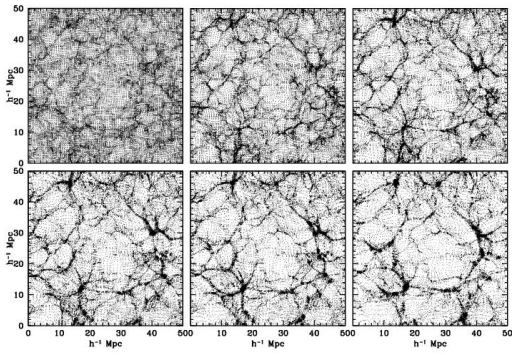

Figure 3: Six frames present the formation of a void at six different time steps according to a 128^3 N-body simulation. The process of the void-in-void is clearly observable in the simulation: small voids are embedded into larger ones forming an underdense region of $25\,h^{-1}Mpc$ diameter[7].

(3) The Hubble flow is the motion of galaxies and of the other cosmic structures due entirely to the expansion of the Universe. From the Hubble flow, Hubble derives the Hubble low

$$v_{rec} = H_0 d$$

where H_0 is the Hubble constant, an expansion parameter, and v_{rec} is the recessional velocity.

3.2 Shape of voids

The first approximation that makes us understand the main voids' features is the one of an evolving and isolated void.
When an underdense region in an Einstein-de Sitter universe reaches an underdensity of $\delta_v = -2.81$[6] it enters the shell-crossing phase where matter outflows from its interior and accumulates near the boundaries with the formation of ridges, that are matter density peaks. When the void evolves into an underdensity of 20% of the global cosmological density, $\delta_v = -0.8$[6], its expansion slows down with respect to the earlier linear expansion. This approximation would be realistic if all the voids could be described as pure and uncompensated bucket shaped voids, but the reality is far different from this approximated theoretical model.
Since voids can not be considered perfectly spherical and isolated objects, Icke[12] proposed an approximation where voids are seen as homogeneous underdense ellipsoids. It is useful to point out that this approximation is only valid for the interior of the region, since its boundaries are characterized by matter density peaks. Although the one of the ellipsoidal model is just an approximation, it is good for the understanding of the main aspects of voids.
According to the homogeneous ellipsoidal model, an object is a cosmic region with an ellipsoidal geometry and with a homogeneous density profile with respect to a uniform density background itself; in the case of the description of voids, ρ_u will be the cosmic density background. If we suppose the general case of a tidal shear directed along the principal axis of the ellipsoid, the subsequent expression for the gravitational acceleration along that axis comes from the equation below:

$$\frac{d^2R_m}{dt^2} = -4\pi G\rho_u(t)\left[\frac{1+\delta}{3} + \frac{1}{2}\left(\alpha_m - \frac{2}{3}\right)\delta\right]R_m - \tau_m R_m + \Lambda R_m \tag{3}$$

We suppose that the ellipsoid is subjected to an external tidal field induced by a matter fluctuation in its neighbourhood[11]. At first sight, it could be a contradiction: it is nearby impossible to have a homogeneous density object and at the same time a density fluctuation; actually this model is self-consistent if we consider just the first approximation.
The total gravitational potential of a homogeneous ellipsoid is given by:

$$\Phi_{tot}(\vec{r}) = \Phi_u(\vec{r}) + \Phi_{int}(\vec{r}) + \Phi_{ext}(\vec{r})$$

There are three quadratic contributions to the total potential.
The first one is the potential distribution of the homogeneous background with cosmic density $\rho_u(t)$, it is given by:

$$\Phi_u(\vec{r}) = \frac{2}{3}\pi G\rho_u(t)(r_1^2 + r_2^2 + r_3^2)$$

where r_1, r_2, r_3 are the coordinates of a mass inside the ellipsoid.
The second contribution is given by the potential field of the ellipsoid:

$$\begin{aligned}\Phi_{int}(\vec{r}) &= \frac{1}{2}\sum_{m,n}\Phi^{int}_{mn}r_m r_n \\ &= \frac{2}{3}\pi G\left(\delta - \rho_u\right)\left(r_1^2 + r_2^2 + r_3^2\right) + \frac{1}{2}\sum_{m,n}T^{int}_{mn}r_m r_n \\ &= \pi G\left(\delta - \rho_u\right)\sum_m \alpha_m r_m^2\end{aligned}$$

where δ is the ellipsoid's density, α_m are the ellipsoidal coefficients and $T^{int}_{m,n}$ is the internal tidal shear tensor.
In the latest passage of the equation the internal tidal shear tensor is cancelled since we consider just spherical perturbation.
The last contribute is the one of the external potential field given by:

$$\Phi_{ext}(\vec{r}) = \frac{1}{2}\sum_{m,n} T^{ext}_{mn} r_m r_n$$

where T^{ext}_{mn} is the external tidal shear tensor.
The Poisson-Newton equation says that

$$\nabla^2\Phi = 4\pi G\rho$$

In the case presented here

$$\Phi_{int} = \pi G\rho \sum_m \alpha_m r_m^2$$

In conclusion, we derive that:

$$\sum_m \alpha_m = 2$$

The gravitational acceleration of a mass point towards the principal axes of the ellipsoid is given by the formula $g = -\nabla\Phi_{tot}(\vec{r})$. Hence:

$$\frac{d^2 r_m}{dt^2} = -\frac{4\pi}{3} G\rho_u r_m(t) - \sum_n \Phi^{int}_{mn} r_n(t) - \sum_n T^{ext}_{mn} r_n(t) \tag{4}$$

It is possible to express the coordinates of the location of the mass element at time t $r_m(t)$ with respect to the initial proper position $r_{k,i}$ through the definition of a spatial matrix R_{mk} dependent on the time: $r_m(t) = \sum_k R_{mk}(t) r_{k,i}$.
Eq.(4) becomes

$$\frac{d^2 R_{mk}}{dt^2} = -\frac{4\pi}{3} G\rho_u R_{mk}(t) - \sum_n \Phi^{int}_{mn} R_{nk}(t) - \sum_n T^{ext}_{mn} R_{nk}(t) \tag{5}$$

Here, we make the assumption that the principal axis of the ellipsoid is aligned with the principal axis of the inertia tensor $I_{i,j}$ in order to prevent the occurrence of the torquing and angular momenta. In the reality of the N-body simulations, it is observed that the strongest tidal field component is aligned among the smallest axis of the ellipsoid, that means a particular shape evolution of voids and other overdense regions.
In a mathematical sense the alignment of the principal axes implies the vanishing of all the off-diagonal elements of the external tidal tensor:

$$T^{ext}_{mn} = T^{ext}_{mm}\delta_{mn}$$

and

$$\sum_n T^{ext}_{mn} R_{nk} = T^{ext}_{mm} R_{mk}$$

The expression of the gravitational acceleration is now given by:

$$\begin{aligned} \frac{d^2 R_m}{dt^2} &= -\frac{4\pi}{3}\rho_u R_{mk} - 2\pi G\delta\alpha_m R_{mk} + 2\pi G\rho_u \alpha_m R_{mk} - T_{mm} R_{mk} \\ &= -2\pi G\left[\alpha_m\delta + \left(\frac{2}{3} - \alpha_m\right)\rho_u\right] R_m - T_{mm} R_m \end{aligned} \tag{6}$$

The only difference between Eq.(3) and Eq.(6) is the fact that the first one takes into account of the influence of the cosmological constant Λ.
Thanks to recent N-body simulations, Icke[13], beside the ellipsoidal model, pointed out that any isolated aspherical underdensity will become more spherical as it expands, in fact the gravitational acceleration is stronger on the shorter axis rather than on the longer one. That means an infall acceleration of matter in overdensity regions that slowly reach the shape of filaments and knots and an outward acceleration for underdensity ones. This acceleration toward the longer axis has the consequence of diminishing the asphericities. Although this tendency has been confirmed by simulations, Platen, van de Weygaert & Jones[14] found out that voids will never be perfectly spherical due to the fact that while expanding, voids will encounter other features of the cosmic web that will modify their shape or they will be subject to external tidal forces.
According to the works by van de Weygaert[6], voids have a prolate shape with axes ratio of the order of $c_1 : c_2 : c_3 \approx 0.5 : 0.7 : 1$.

3.3 Dynamics of voids

The structure and the evolution of voids are related to the tidal forces induced by the large scale environment of the cosmic structures and also to the possibly running up of two expanding voids.
External tidal forces can be so strong that they can make a spherical void expand anisotropically and even collapse, as it is observable in the graph below.
The figure shows two possible ways of evolution of the same initial spherical void. The solid line represents the case of an external tidal force field that makes the void collapse, whereas the dashed line shows the evolution of void if no external force is considered.
Two are the main processes, illustrated in Figure 5, of the evolution of voids: merging and collapse.

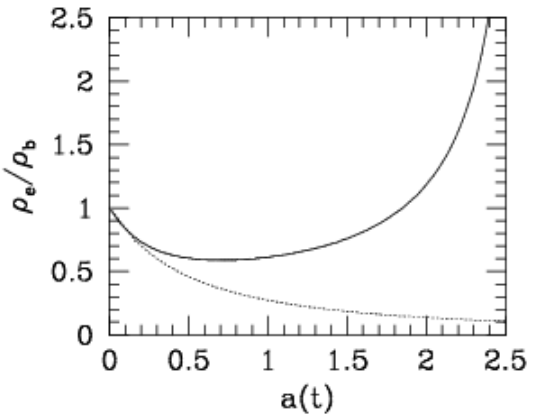

Figure 4: Evolution and collapse of the same initial spherical void. On the x axes there is the evolution parameter, on the y one the initial density of the void ρ_e in unity of the cosmic background density ρ_b[7].

Void merging

As already said, voids appear when the structure formation reaches a non-linear stage; in fact immediately following the Big Bang the Universe was homogeneous and isotropic and the first random field was a nearly random Gaussian field. Since that moment small density fluctuations began to appear and grow and the first density troughs formed.
When two underdense regions meet up, the matter between their boundaries is squeezed up in walls and filaments, and since the velocity of matter escape perpendicular to void's edges is suppressed, we see only tangential motions. After the stage of merging the newborn void starts fading because of the outflow of matter and it reaches the mature

stage as its internal substructure is erased. When a large and a small voids meet up, the result of merging is the absorption of the smaller one by the larger void, that explains why small voids are discarded in the N-body simulations.

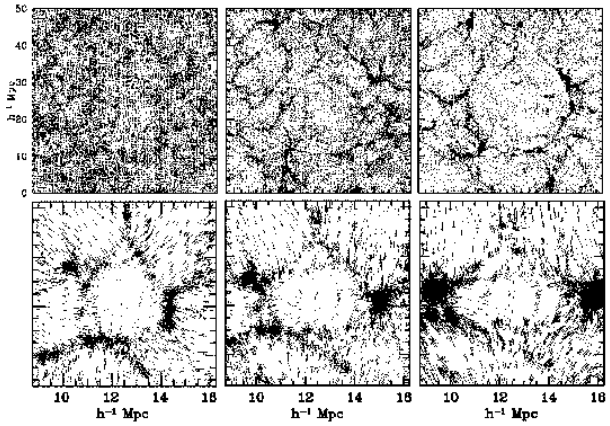

Figure 5: Void merging (top row) and void collapse (bottom row). Each row presents three time steps of evolving void structure in a 128^3 particles N-body simulation of structure formation and collapsing at a(t)=0.1, 0.3, 0.5; in the top row it is presented the formation of a $25\,h^{-1}Mpc$ diameter void according to a void in void process (small voids are involved in larger ones), whereas in the bottom row are presented three voids collapsing due to external tidal shears. The arrows indicate the velocity vectors[7].

Void collapse

The process of collapsing voids is another process responsible for the lack of small voids. In fact, when a small underdense region is embedded in a large overdense one, the collapsing matter squeeze void's edges and it completely vanishes. Also external tidal forces can be the reason of the collapsing of an underdense region within the cosmic pattern.
The process of collapsing highlights the broken symmetry between over/under-density regions, since in the primordial Universe there was a solid difference between clusters of matter and large voids. This underlines the fact that voids represent a pristine environment useful for the inspection of the first epoch of the Universe.

4 Geometric analysis of the Cosmic Web

In the previous Chapters we have introduced the complicated and anisotropic geometry of the Cosmic Web with knots, filaments, walls and voids and this structure is predicted by N-body simulations(4).
Measures of galaxies' redshift allow the mapping of the complicated and interconnected structures of the Cosmic Web, in that sense, galaxies are considered the main tracers of the cosmic structure. Nevertheless, while cosmological theories describe the development of the distribution of matter in terms of continuous density and velocity fields, our knowledge of the cosmic geometry follows from discrete samplings of these fields.
Since both the distribution of galaxies and the particles in a N-body computer simulation are examples of points discretely sampled and with an irregular spatial distribution, we need to translate these discrete objects into a continuous field.
The techniques that should analyse the complex and intricate geometry of the cosmic web with its density variations need not to lose information in terms of spatial resolution and need to trace all the structures in an objective fashion giving the representation of the anisotropic spatial pattern. This far, it has been impossible to extrapolate the totality of the information from the cosmic web, mainly because of the limited mathematical machine possibilities. It is indeed very difficult to quantify and describe all the aspects of the Cosmic Web; the majority of the statistical methods introduced are based on the description of a single aspect of the Cosmic Web. However, these techniques can not identify all the other cosmic structures as well and they are biased towards preconceived notions of their morphology and scale.
Neither general methods nor ad-hoc techniques are able to give an exhaustive description of the Cosmic Web.
It has been proved that maybe the best way to study the large scale geometry of the Universe consists of a tessellation of the space along with an interpolation. In fact, data interpolation represents a more realistic approach because interpolation is independent from specific model assumptions and it is based on the point dependence on its neighbours.
In order to pursue this aim, two main methods have been introduced and tested with success in the field of tessellations: the Voronoi and Delaunay tessellations.
Voronoi and Delaunay tessellations are examples of spatial tessellations, whose potential lies in the ability to divide the space into convex cells that adapt themselves to the local density and geometry of the underlying distribution function of points. Moreover, these two methods are the basis of the *Delaunay Tessellation Field Estimator*, known as DTFE, that highlights and shows essential elements of the cosmic matter distribution, allowing the analysis of large data set through an interpolation (natural neighbour interpolation) of the sampling points.

(4) N-body simulation is an essential instrument in cosmology; it is a computer simulation that allows the study of the formation of the Cosmic Web structures and main features, first of all its non-linearity.

4.1 Spatial tessellations

Spatial tessellations are the main features of the field of Stochastic Geometry and Computational Geometry.
Stochastic geometry is a branch of mathematics that studies all the geometrical structures which can be described by random sets and solves all the problems that arise when we ascribe a probability distribution function to a point sampling.
This is exactly what happens in the astronomical case: there is an inner contrast between the cosmological theories that deal with density and velocity continuous fields and the reality of the observational data coming from the redshift galaxies' surveys or the N-body simulations that provide just discrete samplings of this field.
This is the reason why several stochastic methods have been introduced and largely used in cosmology, yielding the arising of the stochastic geometric field, along with the one of the Computational Geometry.
Computational geometry deals with the research of computational procedures in order to process large data sets.
Within this context, we see the birth of N-body simulations, an example of spatial point process where the points in a constrained astronomical simulation are discretely sampled and have an irregular spatial distribution. Although it is impossible to get all the values at every space point, these methods are useful tools for the study of cosmic matter distribution. Hence, the necessity of finding stochastic instruments and algorithms that will allow the reconstruction of continuous fields from a large set of particle distribution and, as a consequence, the study of these fields principally through interpolations like the *Natural Neighbour Interpolation*.
In this complicated stochastic context, we introduce and analyse random tessellations.
Random tessellations emerge in the process of division of a $\mathbb{R}^d$ space into convex cells; using other words, *random tessellation is an arrangement of polytopes (polygons in 2-D and polyedra in 3-D) fitting together without overlapping in order to cover a d-dimensional space* $\mathbb{R}^d$ *(d=1,2,..) or a subset* $X \subset \mathbb{R}^d$ [8].
But, what is the mathematical translation of random tessellation?
Suppose to have a space $\mathbb{R}^d$ where d is the dimensional value, a tessellation is the division of that space into a set of $\tau = \{X_i\}$ d-dimensional cells $X_i \subset \mathbb{R}^d$ such that, if we consider $\tilde{X}_i$ the interior of the X_i cell:

- The interiors of the cells have to be disjoint:

  $$\tilde{X}_i \cap \tilde{X}_j = \emptyset$$

  for $i \neq j$

- The collection of the cells $\{X_i\}$ is space-filling:

  $$\bigcup_i X_i = \mathbb{R}^d$$

- τ is a countable set of cells:

  $$\#\{X_i \in \tau : X_i \cap B \neq \emptyset\} < \infty$$

  $\forall$ B bounded such that B$\subset \mathbb{R}^d$

The main random spatial tessellations algorithms used to process cosmological data are the Voronoi and the Delaunay tessellations.
These tessellation of a $\mathbb{R}^d$ space constitute the first step in the construction of continuous fields from a particle distribution.
They are largely considered sides of the same medal, since they are each other dual as it is possible to see in the figure below.

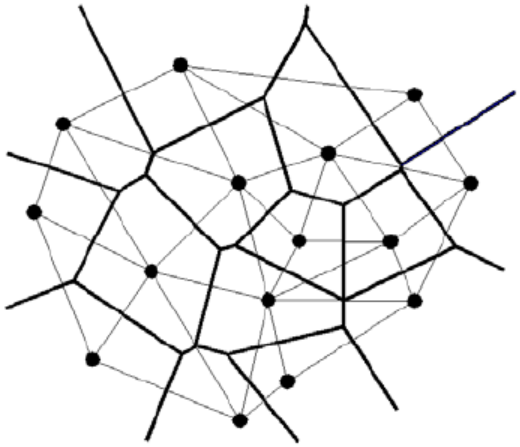

Figure 6: After generating random numbers distributed according to an underlying distribution function (generally a Poissonian distribution) in a square, the next step is the tessellation of the space into convex and disjoint cells. In the figure, the dots are the generated numbers, the solid line represents the tessellation of the space with the Voronoi method, whereas the tenuous one is the tessellation of the 2-dimensional space according to the Delaunay tessellation.

As we will see in the next section, it is possible to infer the Delaunay tessellation from the Voronoi one and vice versa.

Voronoi tessellation

The Voronoi tessellation of a set of point P consists of the division of space into disjunct polyhedra with *each Voronoi polyhedron consisting of the part of space closer to the defining point than any other points*[22].
Suppose a countable set of nuclei (stars or galaxies in the astronomical case) $\{x_i\}$ in $\mathbb{R}^d$, where $\{x_1, x_2, ..., x_d\}$ are the coordinates of the nuclei. The Voronoi region V_i of the nucleus x_i is defined as follows:

$$V_i = \{x | d(x, x_i) < d(x, x_j)\} \quad \forall j \neq i \tag{7}$$

where x is a generic space point and $d(x, y)$ is the Euclidian distance between x and y.
So, the Voronoi region consists of all points nearer to x_i rather than to x_j.
As a consequence, we can say that the boundaries of each Voronoi regions consist of the perpendicular bisectors (2D) or the bisecting planes (3D) of the line segments that connect a general nucleus x_i to all the neighbouring nuclei, defining the *Voronoi polyhedron*.
The 3-dimensional Voronoi tessellation identify four main features: Voronoi cells, Voronoi walls, Voronoi edges and Voronoi vertices.

- Voronoi cells are polyhedra in the 3D Voronoi tessellation of the space, they are the region of space closer to a nucleus $i \in P$ rather than to any other nucleus of the data sampling.
- Voronoi walls are polygons in the 3D Voronoi tessellation of the space, they constitute part of the cell V_i surface since they are composed of point x of the space equally spaced from the nuclei (i, j).
- Voronoi edges are line segments in the 3D Voronoi tessellation of the space and are defined through a set of (i, j, k) nuclei.
- Voronoi vertices are points in the 3D Voronoi tessellation of the space and each of them is defined by a set of four nuclei of the sampling $(i, j, k, l) \in P$. A point of the space is considered a Voronoi vertex if it is equidistant to nuclei (i, j, k, l) and it is closer to them than other set of four nuclei.
  Moreover, each Voronoi vertex is the circumcentre of a Delaunay tetrahedron.

It has not been possible yet to derive an analytical expression for the distribution function of the volumes of Voronoi polyhedra in the case of a Poisson Voronoi tessellation. Nevertheless, Kiang[15] carried out an extensive work on the Voronoi tessellation and he gave a formula that represents a good approximation of the distribution.
According to Kiang, the probability distribution of polyhedra in a d-dimensional space $\mathbb{R}^d$ follows a gamma distribution. The general equation of a gamma function is:

$$\Gamma(x; q) = \frac{q^q x^{q-1} e^{-qx}}{\Gamma(q)}$$

where $x = \frac{V_V}{<V_V>}$, V_V is the size of the Voronoi cell and $< V_V >$ is the average cell size.
The conjecture of Kiang[15] provides that the index has a value q=2d, where d is the dimension of the space tessellation. Finally, the formula of the probability distribution function of the volumes of Voronoi polyhedra is:

$$\Gamma\left(\frac{V_V}{< V_V >}, q\right) = \frac{q^q}{\Gamma(q)} \left(\frac{V_V}{< V_V >}^{q-1}\right) e^{-q\frac{V_V}{<V_V>}} \tag{8}$$

Delaunay tessellations

We know that a set of four nuclei (i, j, k, l) in a 3-dimensional space tessellation uniquely defines a Voronoi vertex, but it also defines a unique tetrahedron, the *Delaunay tetrahedron*. A Delaunay tetrahedron is a simplex element described by a set of four nuclei of the generating set whose circumsphere does not contain any of the other points of the sample.
For the countable set P of points $\{x_i\}$ *in* $\mathbb{R}^d$*, a Delaunay tetrahedron* D_m *is the simplex T defined by (1+d) points* $\{x_{1,i}, ..., x_{i,d+1}\} \in D$ *such that the corresponding circumscribing sphere* $S_m(y_m)$ *with circumcentre* C_m *and radius* R_m *does not contain any other point of P*[8].

$$D_m = T(x_{i,1}, ..., x_{i,d+1}) \quad with\ d(C_m, x_j) > R_m \quad \forall j \neq i1, ..., i(d+1) \tag{9}$$

Now, we want to give the expression of the distribution of Delaunay tetrahedra in d-dimensional space.
If c is the circumcentre of a Delaunay tetrahedron and R is its circumradius, then the

vertices of a Delaunay tetrahedron are $\{c + Ru_i\}$ where $\{u_i\}$ are the unit vectors directed toward the points. The value of the volume V_D of the Delaunay tetrahedron is given by the equation below:

$$V_D = \Delta_d R^d$$

where Δ_d is the volume of the unity simplex $\{u_i, ..., u_d\}$.
Miles[16] and Møller[17][18] found that the distribution of the Delaunay tetrahedra for a Poisson distribution of points in a d-dimensional space $\mathbb{R}^d$ is given by:

$$f_D(D) = f_D(\{u_0, ..., u_d\}, R) = a(n, d)\Delta_d R^{d^2-1} e^{-n\omega_d R^d}$$

where ω_d is the volume of the unity sphere in a d-dimensional space ($\omega_d = 2\pi$ in 2D, $\omega_d = 4\pi$ in 3D) and a(n,d) is a constant depending on number density n and on the dimension value d.

Voronoi and Delaunay characteristics

The comparison between Eq.(7) and Eq.(9), that define the Voronoi polyhedron and the Delaunay tetrahedron, shows the reason why these tessellations are considered each other duals.

- First of all it is possible to infer one from the other and vice versa, since the circumcentre of the Delaunay tetrahedron's circumsphere is a vertex of the Voronoi tessellation. This is a consequence of the definition of Voronoi tessellation because the set of four nuclei that defines the Delaunay tetrahedron are equally distant from the vertex. The following image clearly shows the duality between the geometric elements of these two tessellations.

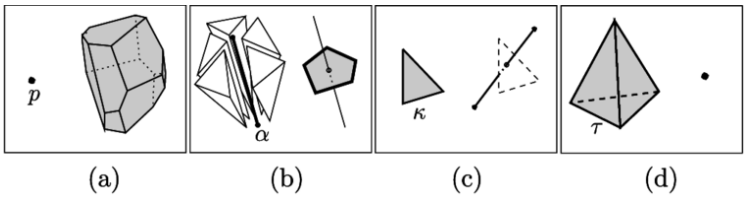

Figure 7: Elements of the Delaunay (left) and Voronoi (right) tessellations. It clearly highlights their duality. For example, frame (d) shows a Delaunay tetrahedron on the left, a geometric simplex that corresponds in terms of Voronoi tessellation to the definition of a Voronoi vertex, a point in the 3D space tessellation.

- The circumsphere of a Delaunay tetrahedron is empty and can not contain any other point of the sampling, as we can infer from the Eq.(9), in fact this point in the circumsphere would be nearer to the circumcentre rather than the other four points defining the Delaunay tetrahedron. And this would be impossible for the circumcentre to be the vertex of all the corresponding Voronoi cells.
  In Figure 8 it is possible to see the dual relationship between Voronoi (solid line) and Delaunay (dashed line) tessellations of a set of nuclei (dots).

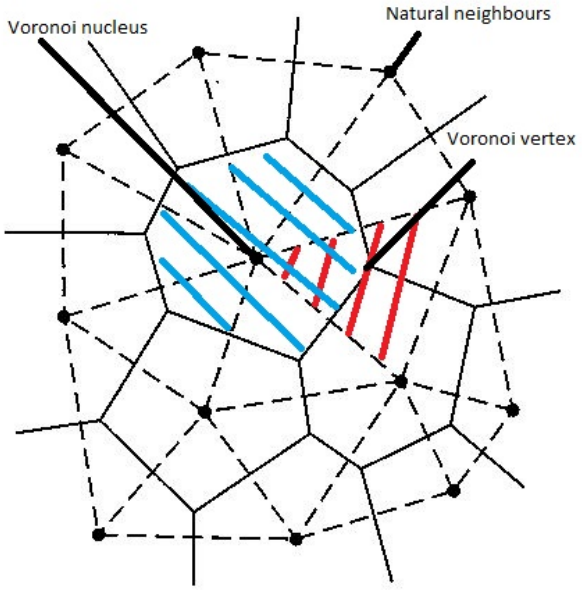

Figure 8: Zoom-in on the Voronoi cells V_i of nucleus i (black dots). The Voronoi cell (blue) at the centre of the figure is surrounded by its related Delaunay triangles (2D, red). Natural Neighbours of the central nucleus are clearly delineated.

Figure 8 also introduce a very important element in term of field reconstruction: *Natural Neighbours*.
A pair of nuclei i and j whose Voronoi cells have a face in common is called contiguous pair and contiguous pair of nuclei are each other's natural neighbour.
We can define natural neighbours two points whose Voronoi cells have a face in common or equally two points connected via a Delaunay tetrahedron.
The main feature of both Delaunay and Voronoi tessellation is their spatial adaptivity, the cells coming from the tessellation of the point distribution adjust themselves to the characteristics of the point distribution as we can clearly see in Figure 9. If the space region is sparsely sampled, the distance between two natural neighbours increase and the distribution of the cells reflect also the anisotropic distribution of matter in the Universe. This is why Delaunay tessellation is considered the major triangulation method in large computer simulations.

4.2 Delaunay Tessellation Field Estimator (DTFE)

Delaunay tessellation field estimator allows the reconstruction of a continuous density field from a point sample through the tessellation of the space with the Delaunay tessellation. DTFE is very useful in the case of large data set, like the one of a cosmological computer simulation; its aim is to obtain local values of the density field through the use of Delaunay tetrahedra for linear interpolation at the point location.
DTFE is largely used in cosmology because it is able to analyse and highlight essential elements of the cosmic matter distribution.

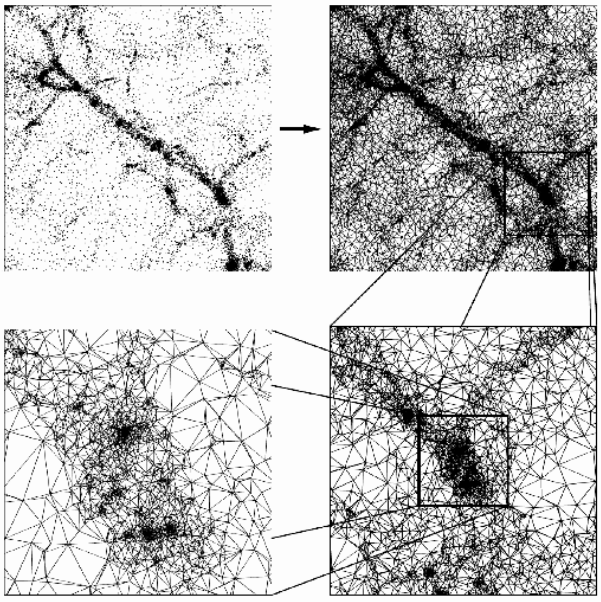

Figure 9: Four frames zooming-in onto the Delaunay Tessellation of a point (star) distribution in and around a filamentary structure of the Cosmic Web. The figure shows the spatial adaptivity of the Delaunay tessellation, whose triangles' distribution adjust itself according to the characteristics of the point distribution[8].

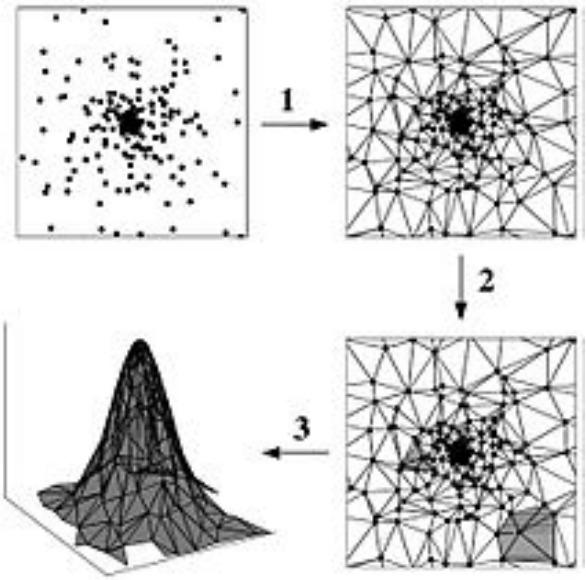

Figure 10: Overview of the main steps of the DTFE procedure. Given a point sample (top left), the first step consists of the construction of its Delaunay tessellation (top right) in order to estimate the density value at each point position as the inverse of its contiguous Voronoi cells (bottom right) and then reconstructing the density field (bottom left) $\rho(\mathbf{x})$ with the assumption that the density varies linearly within each Delaunay simplex (triangle in 2D)[8].

The DTFE reconstruction procedures consists of different steps.

- *Point sample*. Suppose to have a point sample $P = \{\mathbf{x}_1, ..., \mathbf{x}_N\}$ in a d-dimensional (generally, 2 or 3-dimensional) Euclidian space. We can distinguish two cases:

in the first one we have the value of the field $\{f(\mathbf{x}_i), i = 1, 2, ..N\}$ at every point location, in the second one we do not have the values of the field, but they can be obtained thanks to the spatial point distribution. In the case we have the field values, the DTFE uses the Delaunay tessellation for the multidimensional linear interpolation of such measured values; whereas in the case we do not have any information about the field values, Bernardeau & van de Weygaert[19] introduce an extension of the DTFE method. In fact, DTFE is also useful to obtain local values of the field at the location of any point sample in order to reconstruct the underlying density field.

- *Boundary conditions*. The next step consists of assuming boundary conditions. There is a plethora of possibilities, here we enunciate few:
  - Vacuum boundary conditions: there are no points outside the volume sample, in this case Voronoi cells near the boundary will have an infinite extension. This leads to the impossibility of using these cells for a thorough field interpolation since the volume of the DTFE reconstruction is smaller than the volume of the point sample.
  - Periodic boundary conditions: there is a periodic repetition of the point sample around the boundaries, this leads to a toroidal topology of the sample volume. In this case Voronoi ad Delaunay tessellations are both sample volume filling, this is why periodic boundary conditions are very useful in the case of a N-body computer simulation.

- *Delaunay Tessellation*. This is the main step of the DTFE process and consists of the construction of the Delaunay tessellation from the point sample as it is possible to see in Figure 9.

- *Field values point sample*. If we want to extrapolate, for example, the density field value from a point distribution sample we have to use the Voronoi tessellation. Generally, the value of the density field at each point position is the inverse of the volume of the point contiguous Voronoi cell W_i. In the case of a computer N-body simulation, the distribution of the point sample shows an underlying and unbiased density field and the density value in a d-dimensional space is

$$\hat{\rho}(\mathbf{x}_i) = (1 + d)\frac{w_i}{V(W_i)}$$

  where w_i is the weight of point i, usually the mass point.
  In the case of a non-uniform sampling process, when the underlying density function is a selection function $\psi(\mathbf{x})$, varying as function of redshift, depth or sky position, the density estimate for a d-dimensional space is:

$$\hat{\rho}(\mathbf{x}_i) = (1 + d)\frac{w_i}{\psi(\mathbf{x})V(W_i)}$$

- *Field Gradient*. Suppose to be in a Delaunay simplex m of a d-dimensional space. It is important to calculate the value of its field gradient $\hat{\nabla f}|_m$ by solving a set of linear equations for the field values at the position of the (d+1) tetrahedron vertices in order to do an interpolation.
  The requirement in this case is that the field does not strongly fluctuate in the volume sample, because in that case the linear interpolation would not be meaningful.

- *Linear Interpolation*. After the tessellation of the space via Delaunay tessellation, it is convenient to use a multidimensional linear interpolation in order to obtain the value of a generic field $f(\mathbf{r})$ from a discrete point sample. The average value of the field $\hat{f}_{dt}(\mathbf{x})$ at any point position obtained with Delaunay interpolation process is:

$$\hat{f}_{dt}(\mathbf{x}) = \hat{f}_{dt}(\mathbf{x}_i) + \hat{\nabla f}|_m \cdot (\mathbf{x} - \mathbf{x}_i)$$

where $\hat{\nabla f}|_m$ is the linear field gradient that is supposed to be constant within each Delaunay simplex.
We can derive the field gradient from the field values f_i at the vertices location $\mathbf{r}_i$ via the formula:

$$\nabla f = \begin{pmatrix} \frac{\partial f}{\partial x} \\ \frac{\partial f}{\partial y} \\ \frac{\partial f}{\partial x} \end{pmatrix} = A^{-1} \begin{pmatrix} \Delta f_1 \\ \Delta f_2 \\ \Delta f_3 \end{pmatrix} \tag{10}$$

where

$$\Delta x_n = x_n - x_0 \quad for\, n = 1, 2, 3$$

$$\Delta y_n = y_n - y_0$$

$$\Delta z_n = z_n - z_0$$

$$\Delta f_n = f_n - f_0$$

and

$$A = \begin{pmatrix} \Delta x_1 & \Delta y_1 & \Delta z_1 \\ \Delta x_2 & \Delta y_2 & \Delta z_2 \\ \Delta x_3 & \Delta y_3 & \Delta z_3 \end{pmatrix}$$

Once the value of the field gradient ∇f has been determined for each Delaunay tetrahedron, it is possible to derive the field value $\hat{f}(\mathbf{x})$ at the position $\mathbf{x}$ via linear interpolation within the Delaunay tetrahedron.

- *Processing*. This step concerns the production of images from image points and all the operations of smoothing/filtering of these images. For the production of the images from grid points, generally the average field value within each grid-cell is used; however, there is a plethora of approaches to follow that gives a greater accuracy such as the *formal geometrical approach* or the *Monte Carlo approach*, largely discussed in ref. [9].
There are also a wide range of filter techniques, such as the linear filtering of a field $\hat{f}$. The field $\hat{f}$ is filtered by means of a convolution with a filter function $W(x, y)$, giving

$$f_s(\mathbf{x}) = \int dx' \hat{f}(\mathbf{x}') W_s(\mathbf{x}', \mathbf{y}')$$

Filtering methods are very useful in order to obtain a "cleaner" visualization of the image and of its significant pattern, but we have to remember also the inner spatial adaptivity of the Voronoi and Delaunay tessellation, that means a spatial adaptivity of the DTFE density field that is smoothed on the basis of the median value of the densities within contiguous Voronoi cells.

For cosmological purpose, when we want obtain a continuous density field from a large data set, it is necessary the requirement that the extrapolated density field $\rho(\mathbf{x})$ must

guarantee mass conservation. The mass of the point sample should be equal to the mass corresponding to the density field.

$$M = \sum_{i=1}^{N} m_i = \int \hat{\rho}(\mathbf{x}) d\mathbf{x} = M \tag{11}$$

where m_i is the mass of a single sample point. Indeed, the interpolation process should guarantee the mass conservation. However, there is another way to express the mass conservation; the integral of Eq.(11) can be written as the sum over the number of tetrahedron of the volume of polyhedra D_m^+.
How does it come from?
If we consider the space $(\mathbf{x}, \hat{\rho})$, in this space a Delaunay tetrahedron is the base hyperplane of a polyhedron D_m^+. So the mass can be written as

$$M = \sum_{m=1}^{N_T} V(D_m^+)$$

where N_T is the total number of Delaunay tetrahedra.
This volume can be also written as

$$V(D_m^+) = \frac{1}{d+1} \left(\hat{\rho}_{m1} + ... + \hat{\rho}_{m(d+1)}\right) V(D_m)$$

where the set of points $\{m1, m2, ..., m(d+1)\}$ are the nuclei vertices of the Delaunay polyhedron D_m^+. Then, the mass formula becomes:

$$\begin{aligned} M &= \frac{1}{d+1} \sum_{m=1}^{N_T} \left(\hat{\rho}_{m1} + ... + \hat{\rho}_{m(d+1)}\right) V(D_m) \\ &= \frac{1}{d+1} \sum_{i=1}^{N_T} \hat{\rho}_i \sum_{m=1}^{N_{D,i}} V(D_{m,i}) \end{aligned} \tag{12}$$

where $D_{m,i}$ is one of the Delaunay tetrahedra whose nucleus i is a vertex. Since the sum $\sum_{m=1}^{N_{D,i}} V(D_{m,i})$ constitutes the contiguous Voronoi cells W_i of a nucleus i, the Eq.(12) becomes:

$$M = \frac{1}{d+1} \sum_{i=1}^{N_T} \hat{\rho}_i V(W_i)$$

Since mass can be expressed as

$$M = \sum_i m_i$$

the equation of the density values is:

$$\hat{\rho}(\mathbf{x}_i) = (d+1) \frac{m_i}{V(W_i)} \tag{13}$$

Eq.(13) shows that the DTFE density value is proportional to the inverse of the volume of each continuous Voronoi cell, this fact can be also infer from the figure below.

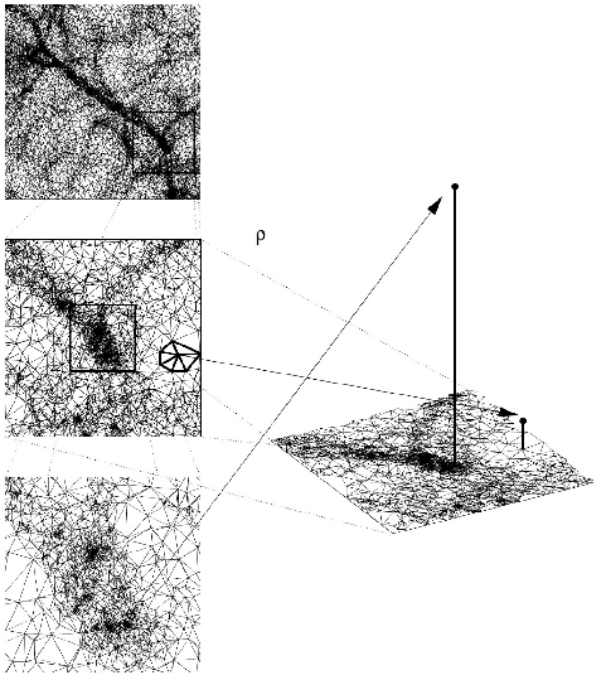

Figure 11: The image shows the inverse correlation between the density value extrapolated via DTFE process and the volume of the contiguous Voronoi cells, specifically in the case of a tessellation in and around a filamentary structure of the Cosmic Web[8].

5 Void Finders

As said in the previous Chapters, voids are considered the main features of the Cosmic Web and we can not understand all the information that comes from such complicate geometric pattern if we do not precisely analyse voids. However, since there is not an objective definition of them, is very difficult to find an algorithm that allows their recognition in a particle distribution. There are several methods, called *Void Finders*, whose aim is to find large underdense regions, each of them with its characteristics and properties.
In this Chapter we briefly discuss two main Void Finders' algorithms: *ZOBOV* and *Watershed Void Finder*.

5.1 Zobov

ZOBOV is a parameter-free void-finding algorithm, whose aim is to find voids from a set of points without strong restrictions on shape or position.
The name ZOBOV comes from an inversion of the parameter-free dark-matter-halo finder, called VOBOZ, with the difference that ZOBOV algorithm looks for density minima instead of density maxima.
First of all, Zobov does not impose any restrictions on voids' shapes, although some theoretical studies show how an extending void in an homogeneous background becomes increasingly spherical and it does not require a filtered or smoothed density field; this means that the algorithm analyses raw data and returns voids of all shapes and types, also dubious ones. Now, ZOBOV method introduces a *statistical significance* for each void in order to distinguish in noisy data real voids from dubious ones.
The following image describes all the main passages of the Zobov algorithm.

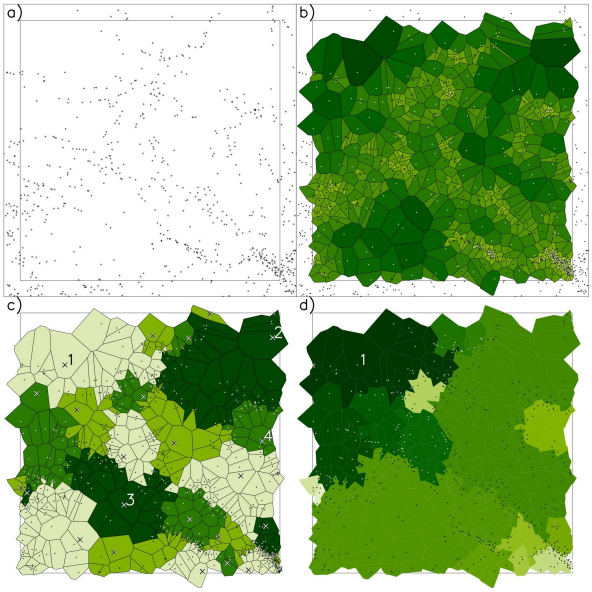

Figure 12: The image presents the four steps of ZOBOV void finding techniques, from a point sample to a space divided into zones with different density value[9].

- *Figure 12(a,b).* After the generation of sampling points distributed according to

a Poissonian distribution, the first step consists of the density estimation at the position of each particle **x** with the Voronoi Tessellation Field Estimator (VTFE) method.
The VTFE is similar to the DTFE, the only difference is that it uses the Voronoi tessellation instead of the Delaunay tessellation. Voronoi tessellation method divides the space into convex cells; if V(i) is the volume of the cell referred to the particle i, the density estimated at the position of this particle is:

$$\rho_i(\mathbf{x}) = \frac{1}{V_i(\mathbf{x})}$$

Voronoi tessellation of the space also provides a natural set of neighbours for each particle that are very useful in the Zobov technique.

- *Figure 12(c).* The second step is called *zoning* and is based on the partition of the particle set into zones around each density minimum. In fact, the ZOBOV algorithm takes each particle and sends it towards regions with the lowest density value, the operation is repeated for each particle until it arrives at a minimum. Two of the key elements of ZOBOV algorithm are: the *minimum's zone*, that is the space region towards which particles flow and the *zone's core*, that is the minimum density value of the zone. After the running of the algorithm, ZOBOV will identify several minimum-density zones, each of them is a void, but we still do not know if they are real or noisy voids.

- *Figure 12(d).* The third and last step gives criteria for the identification of real cosmological voids. Usually the process of finding a zone of deepest density within several other density zones is compared to the behaviour of water into basins. For each zone, we fix the water level to its minimum density value x and then we let this water raise and flow; we see that it starts filling neighbouring zones until it reaches a deeper zone or a zone with a density maximum. The final void corresponding to x is defined as the set of zones containing water before it stops flowing. In the figure we can observe the deepest void that encompasses the whole simulation except for zones with higher density particle. At the end of the algorithm we have a single large void, but this does not mean that ZOBOV does not detect other voids, they are just considered sub-voids. We will see the conditions about voids' boundaries to avoid an infinite extension.

What is the probability that a void v observed via ZOBOV is actually a real void?
We introduce a parameter, $r(v)$, defined as

$$r(v) = \frac{\rho_l(v)}{\rho_{min}}$$

where $\rho_l(v)$ is the density of a particle on a ridge near a void and ρ_{min} is the void minimum density value.
Generally, in an Einstein-de Sitter model of the Universe $\rho_{min} = 0.2\rho_b$, with ρ_b density value of the cosmic background. We know that the Voronoi diagrams applied to a Poisson point distribution function have been studied and understood very well, this is why the parameter $r(v)$ is translated into a probability parameter by comparing it to a Poisson particle distribution.
Suppose that the probability cumulative function $P(r)$ is the fraction of voids of a Poisson

particle distribution with a value of the density contrast greater that r, this probability function for a 3D Poisson simulation can be written as ([9]):

$$P(r) = e^{-5.12(r-1)-0.8(r-1)^{2.8}} \tag{14}$$

If we are in a 2-dimensional space, Eq.(14) becomes:

$$P(r) = e^{-5.12(r-1)} \tag{15}$$

P(r) is the fit function that best describe a set of 256^3 and 256^2 uniformly Poisson distributed particles.
Eq.(14) and Eq.(15) answer the question whether or not a void with such density contrast could arise in a region with that distribution function. Voids in a data set detected by the algorithm can be accepted until r goes below a value where there is no longer agreement between the cumulative probability of Zobov method and the cumulative probability of the major simulations, such as the Millennium Simulation.
We have to introduce boundary conditions to avoid an infinite extension of voids. In fact *the deepest Zobov void in a set of particles will encompass all zones except the one with the highest density ridge separating it from other zones*[9].
Three are the options in order to deal with this problem: the first one is taking the results of Zobov method as they come without changing anything, so the result of the algorithm will be a large void with many sub-voids in it; the second one consists of separating voids according to their statistical significance level previously introduced; the third one consists of using the density contrast of voids and sub-voids to define a probable extension of voids.
Other problems arise when ZOBOV is applied to real data due to observational effects. In fact, this algorithm works very well with boundary conditions, other cases will see the birth of problems since ZOBOV will identify real density minima along with spurious ones, because of the infinite extension of Voronoi cells near the boundaries. It may be a solution to set the boundaries' density values to a value higher than the interior ones or even to introduce a buffer zone around the data set with the average density value.
In Figure 13 is possible to see the result of ZOBOV algorithm applied to the $40h^{-1}$ Mpc AAVFCP cube.

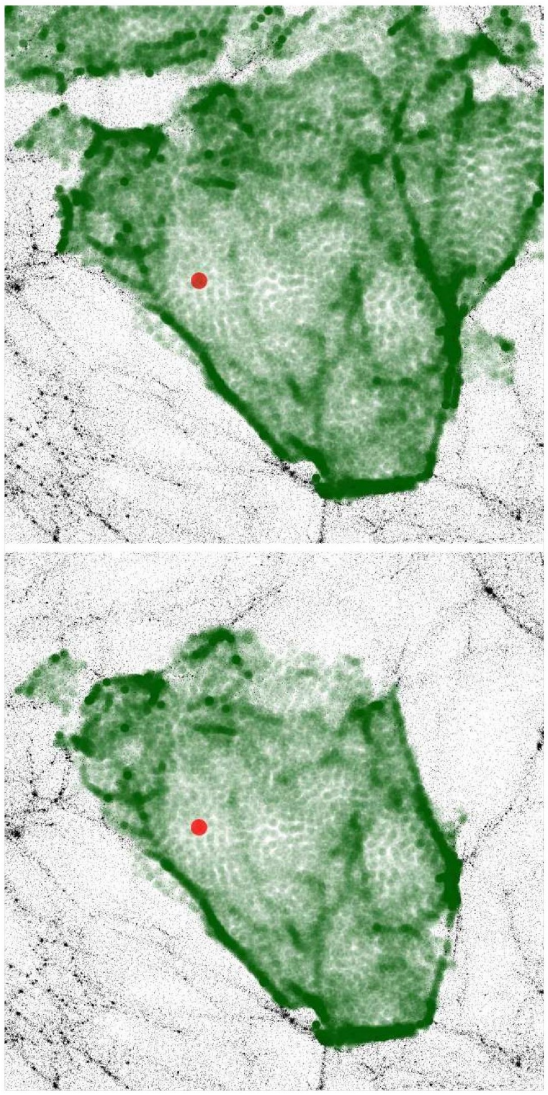

Figure 13: The image presents the detention of a void in the AAVFCP simulation via the ZOBOV algorithm. The red dot in the figure is the minimum density particle in the core of the void and all the green particles are inside that void. In the bottom frame, the void has been separated from its sub-voids according to their significance level[9].

5.2 Watershed Void Finder (WVF)

The WVF technique is very similar to ZOBOV method, they both use tessellations to divide space into convex and disjunct cells and they both are based on the idea of the watershed algorithm; however, WVF algorithm uses DTFE to obtain density field values for each point instead of the VTFE. Moreover, as we will see in this Chapter, the watershed technique uses filtering and smoothing methods applied to the density field, whereas ZOBOV analyse raw data without any filter. The Watershed Void Finding technique is based on the Watershed Transform algorithm first introduced by Beucher & Lantuejoul[20] and Beucher & Meyer[21] that consists of *the segmentation of the image into distinct regions and objects*[10].Its procedure can be observed in Figure 14.

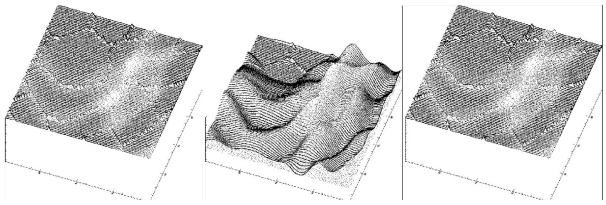

Figure 14: The image presents all the steps of the Watershed process of segmentation of images into distinct regions and objects, underlying the characteristic features of the Cosmic Web[10].

The process of segmentation of the image is based on the idea of water flooding out from a basin (local minima). Suppose to put water in the local minima of the image that has to be segmented (first frame of the figure). We slowly make the water rise and flood as the level continues increasing, when two basins meet up we put a ridge between them, this will be a void boundary (central frame of the figure). Finally, when the water covers the entire volume, we observe a network with regions enclosed into dams. This is the pattern of the Cosmic Web.
There are many advantages in the use of the Watershed algorithm instead of other void finders like ZOBOV. First of all, in a realistic situation of a cosmological data set, the WVF needs just few parameters to be set for filtering out noise and smoothing the density field, but these parameters are based on the data set itself. So, we can consider the algorithm of the WVF an almost-free parameter algorithm. Moreover, it does not introduce a preferred geometry or shape for voids and it naturally introduces closed contours, that means that voids' boundaries' overlap will not be counted. Here we list the steps of the watershed procedure within the cosmological context:

- *DTFE* The first step consists of the division of space into convex tetrahedra via Delaunay tessellation and then define a continuous density field from a discrete point sample. Obviously, the DTFE must guarantee the mass conservation of the sample volume.

- *Grid Sampling* The second step is the sampling of DTFE on a grid; we repeat the process of DTFE many times and then we take the average of the values obtained. We have to choose the optimal grid-size, because it has to show clearly all the features of the Cosmic Web and at the same time avoid the observation of noisy elements, too. Grid-size are usually taken in the order of the mean particle distance.

- *Rank-Ordered Filtering* This step guarantees the removal of noise and all the structures emerged due to noise. In fact, after the definition of density values for each point position via DTFE, these values are filtered via the computation of median and max/min values of the point itself and of its natural neighbours.

- *Contour levels* The image is transformed into a set of discrete levels based on their density values.

- *Field minima* Now, we have to identify the minima. We consider minima of the density field those pixels surrounded by grid-cells with higher density values.

- *Flooding* This step corresponds to the implementation of the Watershed algorithm whose process has already been described in Figure 14.

- *Segmentation* This step involves the definition of voids' boundaries. In fact, when two different basins, that correspond to two different voids in the cosmological case, both reach a pixel of the image, such pixel is considered part of their boundaries. This way, we underline void patches.

- *Hierarchy corrections* The final step consists of the elimination of the segmentations whose boundaries have a density value lower than the typical value of void underdensity $\rho = -0.8$[10].

In Figure 15 it is possible to see the steps of the WVF method applied to a cosmological data set and the results it gives.

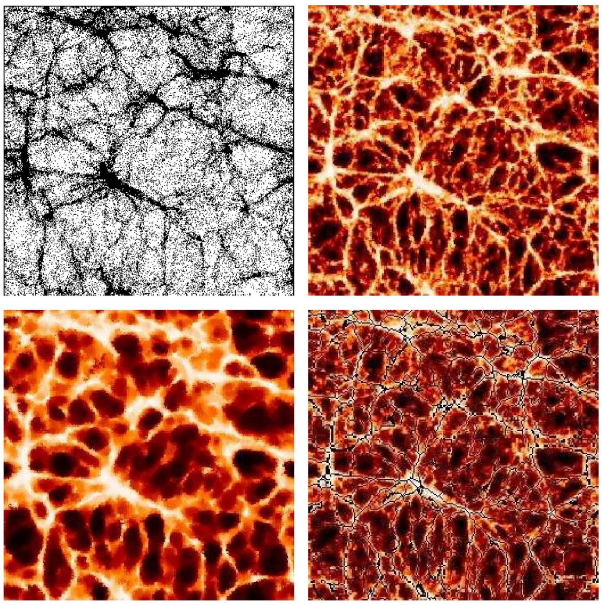

Figure 15: Watershed Void Finding method applied to particles of a ΛCDM simulation. In the bottom-right frame is presented the result of the WVF segmentation with ridges superimposed to the density field.[10].

6 Conclusions

In this thesis we introduced the Cosmic Web, the intricate and interconnected structure of the Universe, and we thoroughly analysed its main aspects, from knots and filamentary structures, to walls and large underdense regions, voids.
We saw how these structures evolve thanks to large data simulations and how matter organises creating underdense regions and overdense ones.
Then, we focused on voids, since their pristine environment is important for the study of the early Universe and density fluctuations. Indeed, voids are manifestation of the cosmic structure formation reaching a non-linear stage.
We saw how pristine density troughs can be considered nursery of the first voids and how voids evolve after an increasingly outflow of matter. We made further approximations, first considering voids almost spherical structures, then introducing the ellipsoidal model and finally, following the works of van de Weygaert, we assumed realistic voids with a prolate shape. Then we talked about their dynamics and how tidal forces are the main responsible of their merging and collapse, contributing to the creation of filamentary structures of the Cosmic Web.
In the third Chapter we introduced tessellation methods and the DTFE technique, useful when we want to compute a continuous density field from a discrete sample of particles or galaxies (in a cosmological case).
Tessellation techniques are, finally, the basis for the developing of void-finding algorithms such as ZOBOV and the Watershed Void Finder. Thanks to these algorithms we were able to reconstruct the Cosmic Web pattern from a set of points coming from computer simulation or from galaxy surveys' observation and we were also able to have an almost exhaustive knowledge of the Universe and its features at Megaparsec scales.

Bibliography

[1] P. A. R. Ade *et al.* [Planck Collaboration], "Planck 2015 results. XIII. Cosmological parameters", Astron. Astrophys. **594**, A13 (2016)

[2] R. P. Kirshner, A. Oemler, Jr., P. L. Schechter and S. A. Shectman, "A million cubic megaparsec void in Bootes", Astrophys. J. **248**, L57 (1981)

[3] V. de Lapparent, M. J. Geller and J. P. Huchra, "A Slice of the universe", Astrophys. J. **302**, L1 (1986)

[4] R. van de Weygaert, N. Libeskind et al, "Tracing the Cosmic Web", preprint arXiv:1705.03021v1 (2017)

[5] R. van de Weygaert & J. R. Bond, "Clusters and the Theory of the Cosmic Web", Lect. Notes Phys. **740**, 335–407 (2008)

[6] R. van de Weygaert, "Voids and the Cosmic Web: cosmic depressions & spatial complexity", IAU Symp. **308**, 493 (2016)

[7] R. van de Weygaert and E. Platen, "Cosmic Voids: structure, dynamics and galaxies", Int. J. Mod. Phys. Conf. Ser. **01**, 41 (2011)

[8] R. van de Weygaert and W. Schaap, "The Cosmic Web: Geometric Analysis", Lect. Notes Phys. **665**, 291 (2009)

[9] M. C. Neyrinck, "ZOBOV: a parameter-free void-finding algorithm", Mon. Not. Roy. Astron. Soc. **386**, 2101 (2008)

[10] E. Platen, R. van de Weygaert and B. J. T. Jones, "A Cosmic Watershed: The WVF Void Detection Technique", Mon. Not. Roy. Astron. Soc. **380**, 551 (2007)

[11] M. Plionis & S. Cotsakis, "Modern Theoretical and Observational Cosmology : Proceedings of the 2nd Hellenic Cosmology Meeting, held in the National Observatory of Athens , Penteli, 19–20 April 2001", Springer Science & Business Media, 166-169

[12] Icke V., Astron. Astrophys. **27**, 1 (1973)

[13] Icke V., Mon. Not. Roy. Astron. Soc. **206**, 1P (1984)

[14] E. Platen, R. van de Weygaert and B. J. T. Jones, "Alignments of Voids in the Cosmic Web", Mon. Not. Roy. Astron. Soc. **387**, 128 (2008)

[15] T. Kiang, "Random Fragmentation in Two and Three Dimensions", Zeitschrift für Astrophysik, **64**, 433 (1966)

[16] R.E. Miles, A synopsis of 'Poisson Flats in Euclidian Spaces'. In: *Stochastic Geometry*, ed. by E.F. Harding, D.G. Kendall (John Wiley, New York 1974) pp. 202-227

[17] J. Møller, Adv. Appl. Prob. **21**, 37 (1989)

[18] J. Møller, Lectures on Random Voronoi Tessellations. In: *Lecture Notes in Statistics*, **87** (Springer-Verlag, New York 1994)

[19] F. Bernardeau and R. van de Weygaert, "A New method for accurate velocity statistics estimation", Mon. Not. Roy. Astron. Soc. **279**, 693 (1996)

[20] S. Beucher and C. Lantujoul, in Proceedings International Workshop on Image Processing, CCETT/IRISA, Rennes, France (1979)

[21] S. Beucher and F. Meyer. Mathematical Morphology in Image Processing, ed. M. Dekker, New York, **12**, 433 (1993)

[22] G. Voronoi, J. reine angew. Math. **134**, 198 (1908)